Label-free detection of human enteric nerve system using Raman spectroscopy: A pilot study for diagnosis of Hirschsprung disease

Katsuhiro Ogawa[a], Yusuke Oshima[a,b,*], Tsuyoshi Etoh[a], Yushi Kaisyakuji[a], Manabu Tojigamori[a], Yasuharu Ohno[c], Norio Shiraishi[d], Masafumi Inomata[a]

[a] *Department of Gastroenterological and Pediatric Surgery, Oita University Faculty of Medicine, 1-1 Hasama, Yufu-city, Oita 879-5593, Japan*
[b] *Faculty of Engineering, University of Toyama, 3190 Gofuku, Toyama-city, Toyama 930-8555, Japan*
[c] *Department of Pediatric Surgery, Oita Children's Hospital, 83-7 Katashima, Oita city, Oita 870-0943, Japan*
[d] *Department of Comprehensive Surgery for Community Medicine, Oita University Faculty of Medicine, 1-1 Hasama, Yufu-city, Oita 879-5593, Japan*

A B S T R A C T

Background: Hirschsprung disease (HSCR) is characterized by the absence of an enteric nerve system (ENS). To remove aganglionosis, bowel reconstruction is only a curative treatment. It is mandatory to identify the extent of aganglionosis during surgery. Raman spectroscopy is a nondestructive chemical analysis technique that provides detailed information regarding molecular vibrations. The purpose of this study is to detect the ENS using Raman spectroscopy in the human intestine for diagnosis of HSCR.
Methods: The Raman spectra of each layer of the gastrointestinal wall were collected from surgical specimens of the human rectum. Based on collected spectral data, principal component analysis was performed to determine the ENS. Subsequently, the Raman spectra of HSCR sections were analyzed.
Results: Molecular structures of the gastrointestinal wall were characterized by Raman spectroscopy. Raman spectroscopy could discriminate between ganglion and muscle layers, and the spectra of the border between muscle layers in the aganglionosis were collagen-associated peaks. Either absence on presence of ENS was also confirmed in HSCR material.
Conclusions: Label-free detection of the ENS was successfully demonstrated using Raman spectroscopy. Since this is a preliminary study, the strategy which may contribute to differentiate between ganglionic and aganglionic segments using noninvasive techniques in HSCR should be evaluated by prospective studies in near future.

1. Introduction

Hirschsprung disease (HSCR) is a developmental disorder of the intrinsic component of the enteric nervous system (ENS) and is characterized by the absence of ganglion in the myenteric and submucosal plexuses of the distal intestine. A segment lacking the ENS (aganglionosis) affects bowel function and quality of life. The incidence of HSCR is approximately 1 in 5000 live-born infants. In most cases, aganglionosis involves the rectum or rectosigmoid but occasionally extends more proximally to the entire colon or a significant amount of the small intestine.

Pathological diagnosis accompanied by invasive tissue collection is essential for diagnosing the presence of the ENS in the gastrointestinal wall. The pathological and clinical features of HSCR vary among patients because of the variable extent of the aganglionic segments. Therefore, it is difficult to accurately determine the length of aganglionosis from the distal to proximal, even in intraoperative histopathological diagnosis. Owing to the difficulty in diagnosis, more than half of the patients with postoperative HSCR experience chronic complications during childhood, including fecal incontinence, constipation, and enterocolitis [1, 2]. Therefore, to improve this poor outcome and to obtain a surgical safety margin containing the distal end of the normal ganglionic segment, a novel technique for intraoperative diagnosis is required in pediatric surgery.

Optical techniques, including fluorescence imaging and Raman spectroscopy, are suitable for medical applications as on-site diagnostic procedures. In particular, Raman spectroscopy may be useful as a label-free modality that provides information regarding molecular structure through the analysis of the small scattering of photons, which is derived from molecular motifs in living tissues. In 1990, Raman spectroscopy was applied for the first time in basic medical research [3]. Thereafter, for the last three decades, the significant progress in optical technology rendered it practical for clinical applications [4–11]. Although Raman spectroscopy has also been utilized for detections in peripheral nerves [12, 13], re-

* Corresponding author at: Department of Gastroenterological and Pediatric Surgery, Oita University Faculty of Medicine, 1-1 Hasama, Yufu-city, Oita 879-5593, Japan

E-mail address: oshima-ehm@umin.ac.jp (Y. Oshima).

ports regarding the identification and observation of the ENS based on Raman spectroscopy are nonexistent. Hence, in this study, we aim to identify the human ENS in normal tissue specimens; subsequently, we evaluate aganglionosis in HSCR using confocal Raman microscopy.

2. Materials and methods

2.1. Sample preparation in human adult normal tissue

Archived human biobanks of surgically resected tissue specimens were provided for this study. This study was approved by the institutional review board of the Faculty of Medicine at Oita University (Approval number: 1471). A square formalin-fixed transverse section of approximately 5 mm of the normal rectal wall was obtained from a rectal cancer resected specimen. The rectal wall tissue was divided into four layers (mucosa, submucosal layer, muscularis propria, and serosa) and subjected to microscopic observation and Raman spectroscopic analysis. Although spectral contamination stemming from formalin must be considered, the effect of formalin fixation can be neglected to characterize the Raman spectral features of each layer and the ENS in the normal rectal wall [14].

2.2. Two-photon microscopy

The tissue section of the normal rectal wall was trimmed using a microslicer (DTK-1000, DOSAKA EM CO., LTD. Kyoto, Japan) and observed using an upright two-photon excitation fluorescence microscopy system (A1RMP, Nikon Corporation, Tokyo, Japan) without dye labeling. The observation protocol and instrumental configuration are described elsewhere [15]. In brief, we used emission filters at 525/50 nm (center wavelength/bandwidth) to obtain the autofluorescence signal from the tissue and a short-pass filter at 492 nm to obtain a second-harmonic generation signal from the collagen fibril. The image acquisition was performed through the raster scanning of a highly focused laser beam during 1 s of exposure per image.

2.3. Raman spectroscopy

Raman spectra were obtained using an in Via Raman Microscope (Renishaw, UK). The excitation laser (532 nm, 4 mW; 785 nm, 40 mW) was focused on the specimen via a $60 \times$ water-immersion objective lens (Olympus LUMPLFL, $60 \times W$, NA=1.0). The exposure times were 30 s (532 nm) and 60 s (785 nm). The diffraction gratings were 1800 lines/mm (532 nm) and 1200 lines/mm (785 nm). The spectral range was 600–1800 cm^{-1} and 2800–3100 cm^{-1}, and the spectral resolution was approximately 1 cm^{-1}. A baseline correction of the obtained Raman spectral data was performed by quartic polynomial curve fitting with GRAMS/AI (Thermo Fisher scientific, Salem, NH, US) prior to principal component analysis (PCA).

2.4. PCA of Raman spectral data

Raman spectral data obtained from the normal rectal wall were statistically analyzed using PCA. Raman spectral datasets were prepared for exploratory data analysis using Sirius 7.1 software (Pattern Recognition Systems AS, Bergen, Norway). In the PCA procedure, the set of observations, which corresponded to the Raman signal intensity at each wavenumber (cm^{-1}) of possibly correlated variables, was transformed into a new set of uncorrelated variables, called principal components (PCs). The PCA classification model was built using the mean-centered data of 24 Raman spectra obtained from 17 different portions on the ganglion in the ENS and

seven portions on the muscularis propria (muscle layer) in all low-frequency spectral regions (600–1800 cm^{-1}).

2.5. Evaluation of aganglionosis in a case of HSCR

A formalin-fixed paraffin-embedded (FFPE) specimen was obtained from a one-year-old girl who underwent a pull-through surgery. The FFPE tissue section with the pathologically proven absence of ganglion cells was cut into approximately 15 μm in thickness and subsequently deparaffinized with xylene and rehydrated with alcohol and water prior to performing a Raman spectroscopic observation without any further treatment. Nine Raman spectra from the HSCR specimen were recorded, which comprised three spectra each from the circular muscle, longitudinal muscle, and the border between the circular and longitudinal muscles where the plexus should be located.

3. Results

3.1. Raman spectra of each layer in the rectal wall

First, to understand the Raman spectral features of the human rectal tissue prior to identifying the ENS, the Raman spectra of the mucosa, submucosa, musclaris propria, and serosa after sharp peeling to expose each layer to the surface were obtained. Subsequently, the Raman spectra were randomly collected at five points in each layer, and the average Raman spectra were calculated and evaluated, as shown in Fig. 1a. The Raman signals in the tissue were assigned as in [16]. The result showed strong peaks at 1004 (Phenylalanine ring breathing mode), 1126 (C–N stretching mode), 1450 (CH$_2$ bending mode), and 1660 cm^{-1} (Amide I) in all layers, which can be assigned to the protein-lipid composition of biological tissues. The Raman spectrum observed in the mucosa showed that the Raman signal of nucleic acid was predominant owing to the abundance of cellular components (Fig. 1b). In addition, collagen-related peaks that originated from the lamina propria were detected in the mucosal layer (Fig. 1b). In the submucosa, the Raman signal originating from lipids was observed clearly, and the peak at 1004 cm^{-1} was relatively weak (Fig. 1c). In the muscularis propria, several peaks related to typical proteins were observed and collagen-related peaks lower than those in other layers were evident (Fig. 1d). In the serosa, intense peaks corresponding to collagen were identified (Fig. 1e).

3.2. Identification of ganglion in ENS by Raman spectroscopy

To identify the ENS via Raman spectroscopy, a further analysis of the muscle layer (muscularis propria) of the normal rectal wall was conducted. Subsequently, we focused on the myenteric (Auerbach's) plexus, which lies between the inner circular muscle and outer longitudinal muscle; it was exposed and observed using a two-photon microscope to clarify the distribution of ganglia in the muscle layer prior to Raman measurement. Fig. 2 depicts two-photon excited autofluorescence (label-free) images captured using a two-photon microscope. A ganglion was clearly observed between the muscle fibers, as well as a neural tract extending from the ganglia (Fig. 2). The ENS was successfully discovered on the muscle layer; therefore, the tissue section was subjected to the identification of the Raman spectral features. Subsequently, Raman spectra were collected from the ganglia and the other portion, which mainly comprised muscle fibers for comparison (data not shown). Fig. 3 shows the average Raman spectra of the ganglion of the ENS. The spectral features were similar to the Raman spectra of the mucosa; this might be because the cellular component was abundant. The peaks at 780 and 828 cm^{-1} were assigned to O-P-O
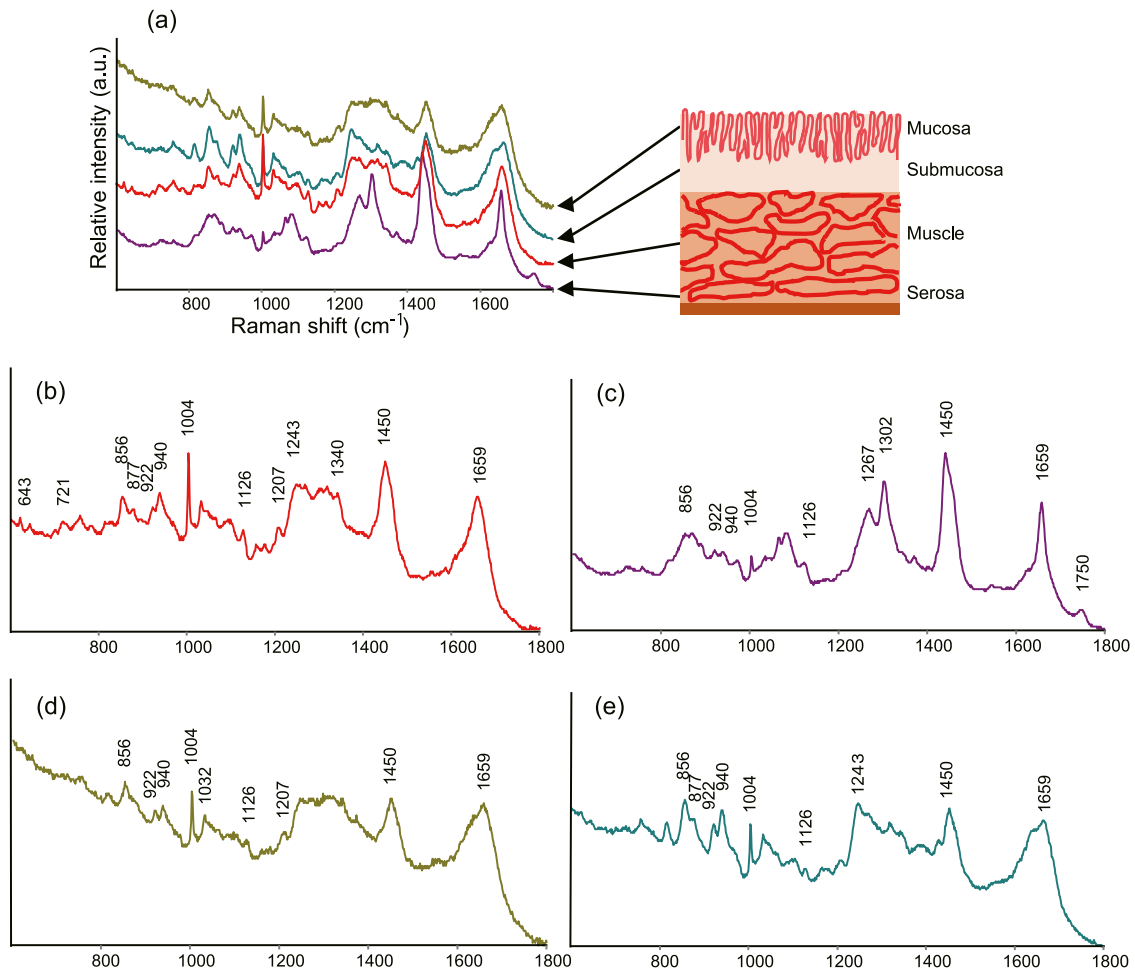
Fig. 1. (a) Raman spectra of each layer in the rectal wall. (b) Mucosa: Raman signals assigned to nucleic acid were observed at 721 (nucleotide peak symmetric choline stretch), 1207 (ring breath mode, DNA [adenine, thymine]), 1243 (asymmetric phosphate stretching modes), and 1340 cm^{-1} (nucleic acid modes indicating the nucleic acid content in tissues). A small peak at 643 cm^{-1} corresponds to the C–C twisting mode of the tyrosine ring. Collagen-related signals were identified at 856 (hydroxyproline), 922 (proline), and 940 cm^{-1} (C–C stretching in protein). (c) Submucosa: Raman peaks at 1302 (CH$_2$ twisting), 1450 (CH$_2$ and CH$_3$ deformation vibrations), 1659 (α-helical structure of amide I), and 1750 cm^{-1} (=C=O stretch) were assigned to lipids. (c) Muscularis propria: Raman signals associated with amino acids, peaks at 856 cm^{-1} (proline, hydroxyproline, tyrosine), as well as 1004 and 1032 cm^{-1} (phenylalanine ring breathing mode) were observed. (e) Serosa: intense peaks corresponding to collagen were identified at 856, 877 (hydroxyproline), 922, and 940 cm^{-1}.
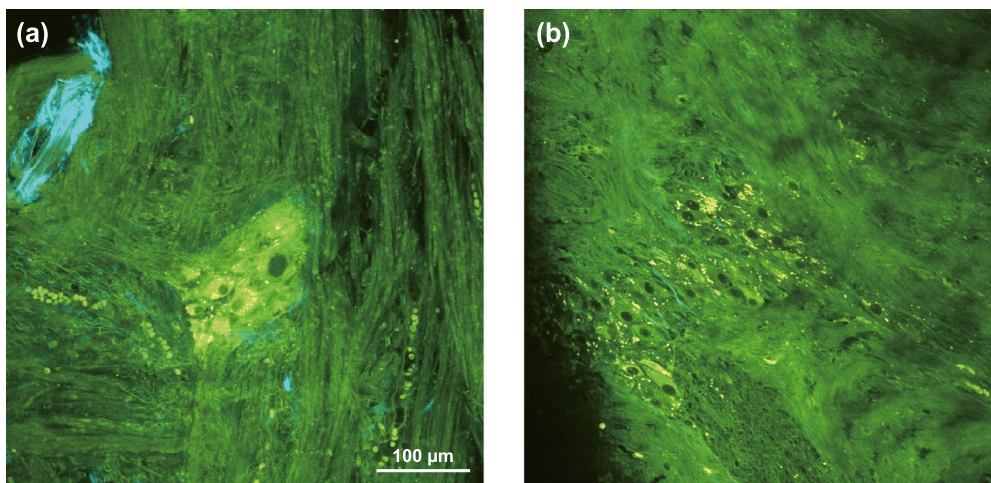

Fig. 2. Two-photon excited autofluorescence images of ganglia and neurons in the muscularis propria. Green color represents autofluorescence signals originating from intrinsic molecules in cells and tissues. Blue color represents the SHG signal emitted from collagen fibers due to the nonlinear optical process. (a) A ganglion was identified in the green bright region surrounding the thinly with blue. (b) Neurons were identified as cellular masses inside the ganglion.
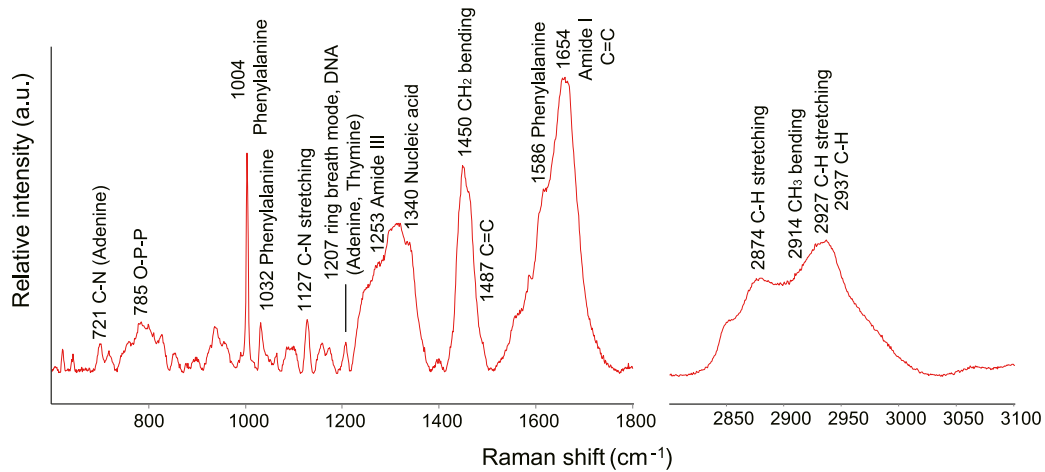
Fig. 3. Average Raman spectra of the ganglion of the ENS.
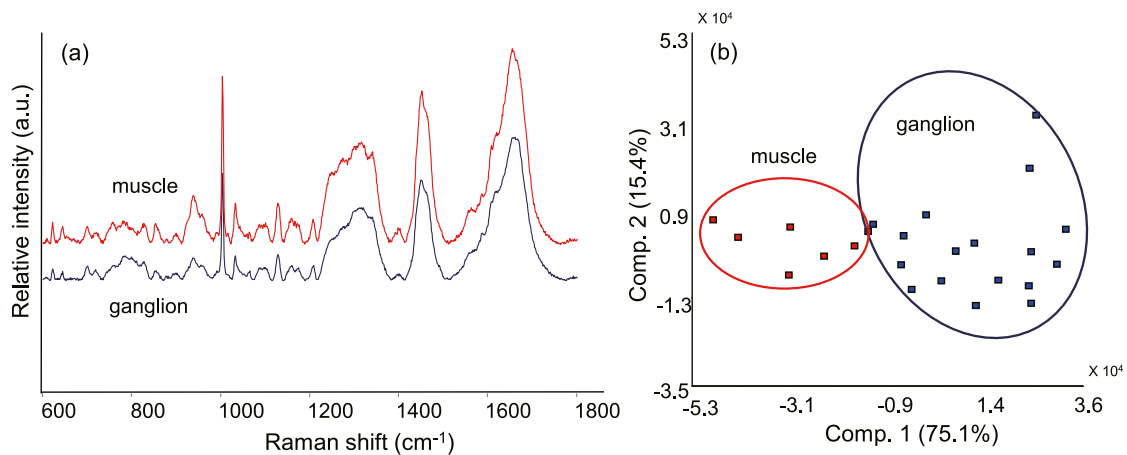

Fig. 4. (a) Average Raman spectra of the ganglion of the ENS and muscle layers. (b) PCA score plots of the datasets for PC1 and PC2.

symmetric and asymmetric stretching modes of nucleic acid, respectively, and the peaks at 1586 cm^{-1} were derived from nucleic acids as well. Peaks at 1127, 1174, 1253, 1449, and 1654 cm^{-1} appeared to be attributed to the C–N stretching, C–H bending, amide III, CH deformation, and amide I modes of protein, respectively.

3.3. Discrimination analysis of Raman spectral data

PCA was applied to analyze the results of the average Raman spectra of the ganglion of the ENS and muscle layers to distinguish the tissue type at each spectral point. PCA score plots for PCs are shown in Fig. 4(b). The datasets for the 17 locations of the ganglion in the ENS and the seven locations of the muscle layers are shown in the plots. The PC1 loading plots were similar to the spectra of the muscle layers. The shape indicates the intensity of each plot owing to the direction of the loading plots. It is difficult to distinguish between the Raman spectra of the ganglion of the ENS and the muscle layers based on a specific peak; additionally, it is assumed that the detection can be performed based on the intensity of each spectrum.

3.4. Evaluation of aganglionosis in HSCR tissue sections

The average Raman spectra obtained from the ENS and muscle fibers were almost similar, as shown in Fig. 4a. An assessment could not be performed by merely comparing these spectra with the naked eye. Hence, to confirm the Raman spectra of the ENS

in HSCR, we performed Raman spectroscopic observations in the FFPE tissue section of a patient with HSCR. Fig. 5 shows the histological mapping of the resected specimen (Fig. 5a) and H&E staining, where the corresponding locations for the Raman measurements are depicted (Fig. 5b). The average Raman spectra of each of the three points of the circular muscle, longitudinal muscle, and the border between the circular and longitudinal muscles where the plexus should be located in the HSCR tissue section are presented in Fig. 6. The three Raman spectra were similar, and the Raman spectra were assigned to aromatic amino acid phenylalanine (1004, 1031, and 1207 cm^{-1}), associated with DNA (1242 and 1340 cm^{-1}) and amide I (1663 cm^{-1}). Compared with the Raman spectra of the circular and longitudinal muscles, the characteristics of the Raman spectra of the border between the circular and longitudinal muscles showed more intense collagen-associated signals (852, 916, and 938 cm^{-1}). In the result, we were able to identify that ENS was missing in the border between the circular and longitudinal muscles using Raman spectroscopy.

4. Discussion

In this study, we developed new diagnostic methods based on optical techniques for the noninvasive detection of the ENS in human rectal intestine using Raman spectroscopy. Furthermore, we detected the extent of aganglionosis, including the transition zone in HSCR, which suggested that it might not only reduce the incidence of postoperative complications, but also improve preopera-
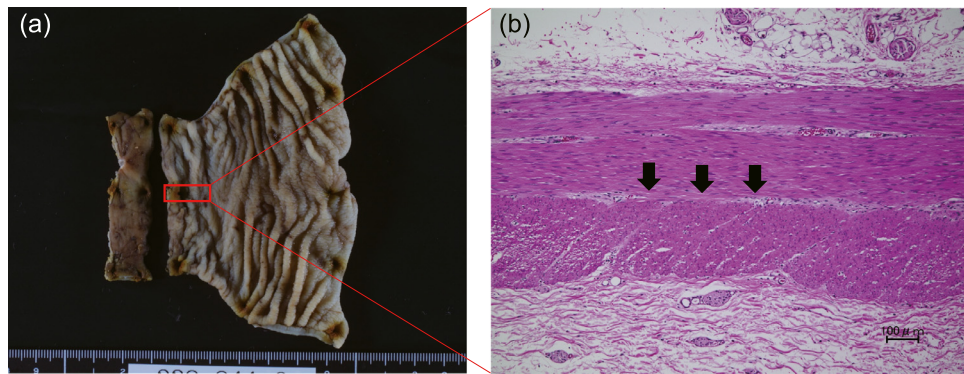
Fig. 5. Histological mapping of resected specimen (a) and H&E-stained sections (b) of HSCR. The two muscle layers of aganglionosis (Inset) that was evidenced by pathological diagnosis, and the border between the circular and longitudinal muscles where the plexus should be located (allow) in the HSCR section are presented in H&E-stained sections.
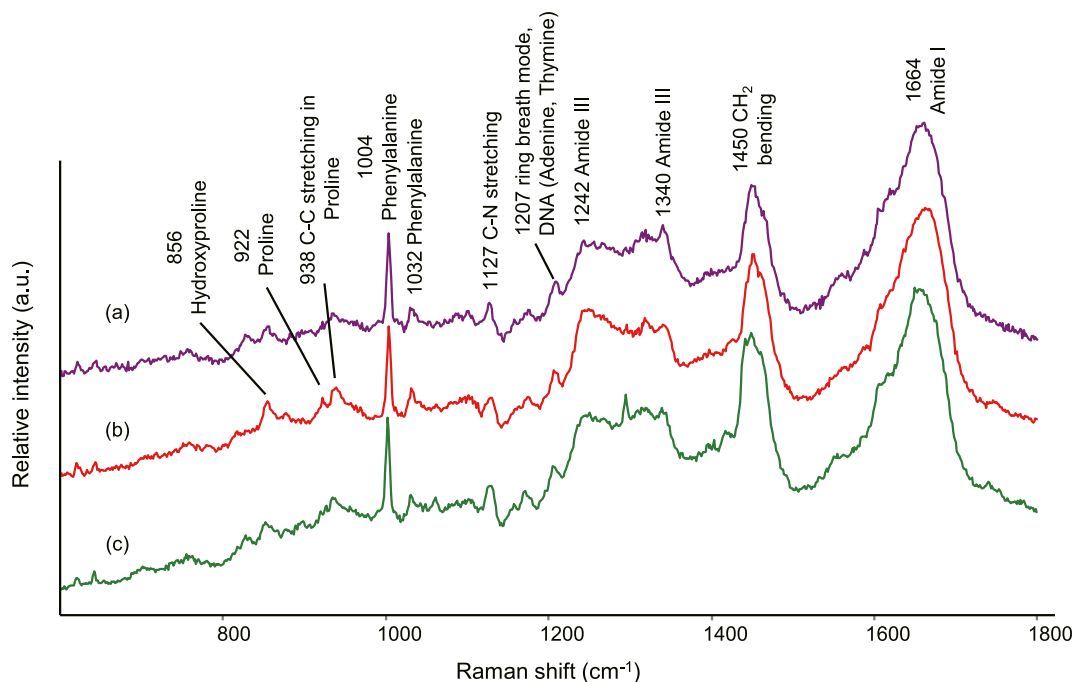

Fig. 6. Average Raman spectra of each of the three points of the circular muscle (a), longitudinal muscle (c), and the border between the circular and longitudinal muscles where the plexus should be located (b) in the HSCR section. Raman spectra of aromatic amino acid phenylalanine (1004 and 1032 cm^{-1}), associated with DNA (1207 cm^{-1}), amide III (1242, 1340 cm^{-1}), and amide I (1664 cm^{-1}) were recorded. The characteristics of the Raman spectra of the border between the circular and longitudinal muscles showed more intense collagen-associated peaks (856, 922, and 938 cm^{-1}).

tive diagnosis of HSCR. Raman techniques are noninvasive and do not require treatments such as drug administration. Hence, these techniques are particularly useful for children.

We focused on Raman spectroscopy in this study as it is a breakthrough in minimally invasive medical technology. Raman spectroscopy provides information regarding molecular vibrations that are strongly related to the molecular structures of tissues. The spectral analysis of the unique "fingerprint" Raman spectrum allows us to identify biological structures of tissue species via molecular vibrations [17]. Recently, Raman spectroscopy has attracted particular interest in the medical field, such as in cancer diagnosis, including esophageal cancer, gastrointestinal cancer, skin cancer, breast cancer, lung cancer, and brain cancer [4, 9, 18–21]. Other studies have also demonstrated that it is not necessary to perform tissue staining in pathological diagnosis using Raman spectroscopy [6, 22, 23]. Furthermore, it has been proven in previous papers that the effect of formalin fixation has little effect to characterize the Raman spectral features [14]. Meanwhile, Minamikawa

et al. [12] and Kumamoto et al. [13] reported the detection of nerves using Raman spectroscopy for nerve-sparing surgery. They demonstrated the distinction of peripheral nerves and their adjacent tissues, such as adipose tissues, collagenous tissues, and skeletal muscles using PCA-based discriminant analysis with representative Raman spectra. Moreover, Hashimoto et al. [24, 25] classified the spectral change of live growing neurons and distinguished between intact excitatory and inhibitory neuronal cells using Raman analysis. However, as studies that focus on the human ENS using human materials are nonexistent, we therefore confirmed the evidence of the human ENS in this study.

It is important to understand the possibility of detecting neurons using Raman spectroscopy because the ENS is characterized by ganglia and nerve tracts that form mesh-shaped nerve networks within the walls of the gastrointestinal tract [26]. When detecting the ENS in the wall of the gastrointestinal tract, we assumed that it is easier to identify ganglia where nerve cells gathered rather than based on fine nerve bundles. Additionally, the characteristics

of HSCR include an abnormal increase in extrinsic nerve fibers in the muscularis mucose to the lamina propria [27]. These extrinsic nerve fibers extend inside the submucosal and myenteric layer as thick nerve bundles that contain no neuronal bodies. In other words, we must determine the Raman spectra of not nerve bundles but ganglia, where nerve cells gather in the ENS because of the detection of aganglionosis extent, including the transition zone in HSCR. Thus far, reports regarding the Raman spectra of cultured neurons have been published [24, 25]; however, those regarding the Raman spectra of ganglia inside the wall of the gastrointestinal tract are nonexistent. First, we attempted to peel off between the inner circular muscle and outer longitudinal muscle to expose the plexus after treatment by incubating the colon tissues with 8 N HCl at 70 °C. Although the degeneration of tissues were strong owing to the action of high-temperature HCl when removing connective tissue components using this method, an accurate Raman spectrum could not be measured. This implied that the chemical digestion method was not suitable for Raman spectroscopy because it destroyed the molecular composition. Therefore, we used a microslicer and two-photon microscopy as described above. Consequently, we detected the ganglia of the ENS distributed among the inner circular muscle and outer longitudinal muscle. As a characteristic of the Raman spectra of the ganglia inside the wall of the gastrointestinal tract, strong DNA was observed at 785 cm^{-1}. This indicates that the amount of DNA per tissue volume was relatively higher in the ganglia than in the surrounding muscle. The DNA peak may be one of the candidates of the merkmal for identifying the existence of the ENS in the muscle layer; however, the Raman signal of the DNA including the 785 cm^{-1} peak was not specific for the ganglia. In addition, both the ganglia and muscle exhibit numerical common peaks derived from typical tissue and cellular components, such as lipids and proteins, and they exhibited similar shapes. To distinguish the ganglia from the muscle more accurately, multivariate analysis PCA should be performed on the Raman spectral data. The PCA score plot of ganglia and muscle layers indicated a good separation and demonstrated the high potential of Raman spectroscopy for discriminating between ganglia and muscle layers.

Based on these results, a section of aganglionosis in HSCR was analyzed via Raman spectroscopy for clinical use. The Raman spectra of the border between the circular and longitudinal muscles in the aganglionosis showed more intense collagen-associated signals that might indicate fibrous septa or the presence of hypertrophic nerve bundles. According to these results, to find the ENS buried in the muscle layer, we first searched for a layer in the muscle layer where a spectrum was related to collagen-associated peaks, and then determined whether a spectrum related to the DNA can be detected in that layer. It was suggested that normal and aganglionosis can be distinguished. Moreover, by the rate of the spectrum related to the DNA in that layer, the detection of the transitional zone might be possible. To prove this hypothesis, it is necessary to collect pieces of HSCR specimens that are not paraffin-embedded but formalin-fixed specimens or fresh samples in the future. Limitation of this study, Raman spectroscopy was performed only on the lesions in HSCR specimens due to consideration of the preservation of the materials. On the other hand, the characteristics in Raman spectrum of the normal part of the intestinal tract is shown by the data obtained from adult rectum. As future work, it is necessary to accumulate more Raman spectral data in HSCR specimens, because comparison of lesion and normal areas in the same specimen is essential.

For the clinical application of Raman spectroscopy, we are currently considering its introduction into endoscopic Raman spectroscopy and laparoscopic Raman spectroscopy. As for the former, many reports have been published that aimed at the diagnostic modality for esophageal, gastric, and colonic pathologies [10, 28–31]. If the ENS can be identified using endoscopic Raman spectroscopy, it can then be used not only for the intraoperative border-line diagnosis of aganglionosis, but also for definitive diagnoses of HSCR, which can replace invasive rectal mucosal biopsy. However, endoscopic Raman spectroscopy is currently limited by its narrow measurement range and its ability to measure only the surface of tissues, such as the epithelium. That means the new modality adding onto colonoscope or laparoscope is still needing far way to go. As a practical matter, for the ENS to exist inside the wall of the gastrointestinal tract, incorporation of advanced techniques for measuring deeper tissues, such as spatially offset Raman spectroscopy [26], must be considered in the future.

5. Conclusion

This study demonstrated the usefulness of Raman spectroscopy in identifying the ENS in the human intestinal wall as a pilot study for intraoperative diagnosis. The possibility of detecting the extent of aganglionosis was suggested, including the transition zone in HSCR disease. In this study, Raman spectroscopy is thoroughly adjunctive for pathological diagnosis, but we believe that the clinical use of this technique will contribute to the reduction of complications as much as possible. Therefore, we are now conducting a multicenter prospective study to confirm the feasibility of Raman spectroscopy for diagnosis in HSCR. Endoscopic Raman spectroscopy may be a novel and noninvasive tool for the clinical diagnostic of the human ENS. Considering the current limitations, further studies are required for future clinical applications.

References

[1] Rintala RJ, Pakarinen MP. Outcome of anorectal malformations and Hirschsprung's disease beyond childhood. Semin Pediatr Surg 2010;19(2):160–7.

[2] Wester T, Granstrom AL. Hirschsprung disease-Bowel function beyond childhood. Semin Pediatr Surg 2017;26(5):322–7.

[3] Puppels GJ, de Mul FF, Otto C, Greve J, Robert-Nicoud M, Arndt-Jovin DJ, et al. Studying single living cells and chromosomes by confocal Raman microspectroscopy. Nature 1990;347(6290):301–3.

[4] Huang Z, McWilliams A, Lui H, McLean DI, Lam S, Zeng H. Near-infrared Raman spectroscopy for optical diagnosis of lung cancer. Int J Cancer 2003;107(6):1047–52.

[5] Haka AS, Volynskaya Z, Gardecki JA, Nazemi J, Lyons J, Hicks D, et al. In vivo margin assessment during partial mastectomy breast surgery using raman spectroscopy. Cancer Res 2006;66(6):3317–22.

[6] Krafft C, Codrich D, Pelizzo G, Sergo V. Raman and FTIR microscopic imaging of colon tissue: a comparative study. J Biophotonics 2008;1(2):154–69.

[7] Oshima Y, Shinzawa H, Takenaka T, Furihata C, Sato H. Discrimination analysis of human lung cancer cells associated with histological type and malignancy using Raman spectroscopy. J Biomed Opt 2010;15(1):017009.

[8] Duraipandian S, Sylvest Bergholt M, Zheng W, Yu Ho K, Teh M, Guan Yeoh K, et al. Real-time Raman spectroscopy for in vivo, online gastric cancer diagnosis during clinical endoscopic examination. J Biomed Opt 2012;17(8):081418.

[9] Ishigaki M, Maeda Y, Taketani A, Andriana BB, Ishihara R, Wongravee K, et al. Diagnosis of early-stage esophageal cancer by Raman spectroscopy and chemometric techniques. Analyst 2016;141(3):1027–33.

[10] Lin K, Wang J, Zheng W, Ho KY, Teh M, Yeoh KG, et al. Rapid fiber-optic Raman spectroscopy for real-time in vivo detection of gastric intestinal metaplasia during clinical gastroscopy. Cancer Prevent Res (Philadelphia, Pa) 2016;9(6):476–83.

[11] Pence I, Mahadevan-Jansen A. Clinical instrumentation and applications of Raman spectroscopy. Chem Soc Rev 2016;45(7):1958–79.

[12] Minamikawa T, Harada Y, Takamatsu T. Ex vivo peripheral nerve detection of rats by spontaneous Raman spectroscopy. Sci Rep 2015;5:17165.

[13] Kumamoto Y, Harada Y, Tanaka H, Takamatsu T. Rapid and accurate peripheral nerve imaging by multipoint Raman spectroscopy. Sci Rep 2017;7(1):845.

[14] Lopes PC, Moreira JA, Almeida A, Esteves A, Gregora I, Ledinsky M, et al. Discriminating adenocarcinoma from normal colonic mucosa through deconvolution of Raman spectra. J Biomed Opt 2011;16(12):127001.

[15] Sagawa N, Oshima Y, Hiratsuka T, Kono Y, Etoh T, Inomata M. Role of increased vascular permeability in chemotherapy-induced alopecia: in vivo imaging of the hair follicular microenvironment in mice. Cancer Sci. 2020.

[16] Rehman IU, Movasaghi Z, Rehman S. Vibrational spectroscopy for tissue analysis. UK: CRC Press; 2012.

[17] Harada Y, Takamatsu T. Raman molecular imaging of cells and tissues: towards functional diagnostic imaging without labeling. Curr Pharm Biotechnol 2013;14(2):133–40.

[18] Hsu CW, Huang CC, Sheu JH, Lin CW, Lin LF, Jin JS, et al. Differentiating gastrointestinal stromal tumors from gastric adenocarcinomas and normal mucosae using confocal Raman microspectroscopy. J Biomed Opt 2016;21(7):75006.

[19] Nijssen A, Bakker Schut TC, Heule F, Caspers PJ, Hayes DP, Neumann MH, et al. Discriminating basal cell carcinoma from its surrounding tissue by Raman spectroscopy. J. Invest. Dermatol. 2002;119(1):64–9.

[20] Frank CJ, Redd DC, Gansler TS, McCreery RL. Characterization of human breast biopsy specimens with near-IR Raman spectroscopy. Anal Chem 1994;66(3):319–26.

[21] Desroches J, Jermyn M, Mok K, Lemieux-Leduc C, Mercier J, St-Arnaud K, et al. Characterization of a Raman spectroscopy probe system for intraoperative brain tissue classification. Biomed Opt Express 2015;6(7):2380–97.

[22] Gaifulina R, Maher AT, Kendall C, Nelson J, Rodriguez-Justo M, Lau K, et al. Label-free Raman spectroscopic imaging to extract morphological and chemical information from a formalin-fixed, paraffin-embedded rat colon tissue section. Int J Exp Pathol 2016;97(4):337–50.

[23] Krafft C, Ramoji AA, Bielecki C, Vogler N, Meyer T, Akimov D, et al. A comparative Raman and CARS imaging study of colon tissue. J Biophotonics 2009;2(5):303–12.

[24] Hashimoto K, Kudoh SN, Sato H. Analysis of the developing neural system using an in vitro model by Raman spectroscopy. Analyst 2015;140(7):2344–9.

[25] Hashimoto K, Andriana BB, Matsuyoshi H, Sato H. Discrimination analysis of excitatory and inhibitory neurons using Raman spectroscopy. Analyst 2018;143(12):2889–94.

[26] Furness JB, Callaghan BP, Rivera LR, Cho HJ. The enteric nervous system and gastrointestinal innervation: integrated local and central control. Adv Exp Med Biol 2014;817:39–71.

[27] Meier-Ruge W, Lutterbeck PM, Herzog B, Morger R, Moser R, Schärli A. Acetylcholinesterase activity in suction biopsies of the rectum in the diagnosis of Hirschsprung's disease. J Pediatr Surg 1972;7(1):11–17.

[28] Garai E, Sensarn S, Zavaleta CL, Loewke NO, Rogalla S, Mandella MJ, et al. A real-time clinical endoscopic system for intraluminal, multiplexed imaging of surface-enhanced Raman scattering nanoparticles. PLoS One 2015;10(4):e0123185.

[29] Sharma N, Takeshita N, Ho KY. Raman spectroscopy for the endoscopic diagnosis of esophageal, gastric, and colonic diseases. Clin Endosc 2016;49(5):404–7.

[30] Jeong S, Kim YI, Kang H, Kim G, Cha MG, Chang H, et al. Fluorescence-Raman dual modal endoscopic system for multiplexed molecular diagnostics. Sci Rep 2015;5:9455.

[31] Kim HH. Endoscopic Raman spectroscopy for molecular fingerprinting of gastric cancer: principle to implementation. Biomed Res Int 2015;2015:670121.